Journal of Catalysis 260 (2008) 315–328

Contents lists available at ScienceDirect

Journal of Catalysis

www.elsevier.com/locate/jcat

# Adsorption and reaction of $NO_2$ on ordered alumina films and mixed baria–alumina nanoparticles: Cooperative versus non-cooperative reaction mechanisms

Aine Desikusumastuti, Thorsten Staudt, Markus Happel, Mathias Laurin [1], Jörg Libuda *

*Lehrstuhl für Physikalische Chemie II, Friedrich-Alexander-Universität Erlangen-Nürnberg, Egerlandstr. 3, D-91058 Erlangen, Germany*

ARTICLE INFO

*Article history:*
Received 26 March 2008
Revised 22 September 2008
Accepted 22 September 2008
Available online 31 October 2008

*Keywords:*
Nitrogen dioxide
Barium oxide
Aluminum oxide
Supported model catalysts
NSR catalysts
Scanning tunneling microscopy
IR reflection absorption spectroscopy
Molecular beams

ABSTRACT

In order to obtain insights into the mechanism and kinetics of adsorption and reaction of $NO_2$ on aluminum and barium oxide surfaces, we have performed systematic adsorption experiments on single-crystal-based model materials. As a model surface, we use BaO containing nanoparticles grown by physical vapor deposition (PVD) of Ba under ultrahigh vacuum (UHV) conditions on an ordered $Al_2O_3$ film on NiAl(110) and subsequent oxidation and annealing. The growth behavior, the morphology and the chemical composition of the three-dimensional mixed barium aluminum oxide particles ($BaAl_{2x}O_{1+3x}$) formed via this procedure have previously been characterized by scanning tunneling microscopy (STM) and high-resolution photoelectron spectroscopy (HR-PES). In order to monitor adsorption and reaction processes on these systems, we perform time-resolved infrared reflection absorption spectroscopy (TR-IRAS) during exposure to a molecular beam (MB) of $NO_2$. In a first step, the interaction of $NO_2$ with the $Al_2O_3$/NiAl(110) model support is probed. At 100 K, only molecular adsorption occurs in form of the $D_{2h}$ dimer ($N_2O_4$) in all coverage regions from the submonolayer up to multilayers. At 300 K, a slow surface reaction occurs, initially leading to the formation of surface nitrites and, subsequently, of surface nitrates in bridging adsorption geometry. On the $BaAl_{2x}O_{1+3x}$ particles on $Al_2O_3$/NiAl(110), $NO_2$ shows a very different and strongly temperature-dependent behavior. At 100 K, molecular adsorption of the $D_{2h}$ dimer ($N_2O_4$) is accompanied by a highly efficient reaction channel, leading to the formation of surface nitrites and nitrates. With the surface temperature increasing to 300 K, however, the reaction probability decreases by several orders of magnitude. In contrast to reaction at 100 K, surface nitrites in flat-lying adsorption geometry are the only primary product, indicating a temperature-dependent change in the reaction mechanism from a cooperative to a non-cooperative pathway. With increasing exposure, the nitrite coverage increases and, finally, the surface nitrites are converted into bridging and monodentate surface nitrates. The latter reaction shows a complex kinetics, including an initial induction period. For temperatures of 400 K and above, nitrate formation becomes more efficient, eventually resulting in the formation of ionic nitrates. The vibrational properties of these ionic species sensitively depend on the reaction temperature, indicating the formation of well-defined structures in a narrow temperature interval around 500 K. The mechanism of the $NO_x$ storage process and the vibrational assignments of the related surface species are critically discussed on the basis of the present results.



## 1. Introduction

Typical heterogeneous catalysts are highly complex materials, which are optimized under static reaction conditions [1]. In contrast, the idea of storage catalysis is completely different. It is based on the accumulation of a specific intermediate by a storage material and subsequent release upon a change in reaction temperature or reactant partial pressures. The additional freedom provided by this concept may open up new possibilities toward tailoring the selectivity and activity of catalyst materials. From the point of view of application, storage catalysts have proven to be particularly successful in emission control. One example is provided by oxygen storage compounds (OSC) which have helped to substantially improve the performance of the conventional three-way catalysts (see e.g. [2,3]). Here, the ceria-based OSC material stores and releases oxygen, thus making it easier to sustain stoichiometric conditions during catalytic conversion under the dynamically changing operation conditions of a combustion engine.

* Corresponding author. Fax: +49 9131 8528867.
*E-mail address:* libuda@chemie.uni-erlangen.de (J. Libuda).
[1] Present address: Research Centre for Spectrochemistry, The University of Tokyo, Hongo, Tokyo 113-0033, Japan.

0021-9517/$ – see front matter 
doi:10.1016/j.jcat.2008.09.020

In this work, we focus on a second example from the field of exhaust gas aftertreatment, which is the $NO_x$ storage and reduction (NSR) catalyst [4]. NSR catalysis represents one possible key concept for the reduction of $NO_x$ exhaust streams produced under lean-burn conditions [5]. Lean-burn engines, i.e. combustion engines which are operated under air-rich condition, have substantially better fuel and $CO_2$ efficiency. However, they may generate problems with respect to the emission of toxic gases, in particular $NO_x$. From a chemical point of view, it is easy to conceive that it is inherently difficult to catalytically reduce $NO_x$ in the strongly oxidizing exhaust gas environment under lean conditions. The NSR concept circumvents this problem by storing $NO_x$ in form of $Ba(NO_3)_2$ during lean operation periods, which are followed by release and reduction of $NO_x$ during short fuel-rich operation cycles. Although NSR catalysts have recently been successfully commercialized, a number of practical problems persist, such as for example irreversible poisoning of the storage material, deactivation, sintering and difficulties in tuning the temperature windows of storage and release (see e.g. [6]).

From the point of view of applied catalysis, the NSR concept has attracted considerable attention after first being suggested by Toyota Co. in 1996 [4]. However, introducing the storage component adds another dimension of complexity to the catalyst material, and, as a result, the underlying reaction mechanism and their microkinetics are only poorly understood at the molecular level [5]. Currently, the discussion involves various aspects including, for instance, the role and reactivity of different Ba-related species, the mechanism of nitrate formation, the role of surface transport and spillover processes, the role of oxidation and reaction of the noble metal component and the role and mechanism of restructuring and poisoning processes (see e.g. [5–11] and references therein).

One strategy toward a molecular level understanding of the underlying mechanisms and kinetics is based on the development of single-crystal-based model catalysts [12–14]. These models allow us to introduce certain aspects of real catalysts, without having to deal with their full complexity. In addition, we can take advantage of the full spectrum of surface science experimental methods. For many supported catalysts, this strategy has been proven to be rather successful [14–18].

The development of model systems for NSR catalysts, however, is still in its very infancy, and little work has been published yet. A first example stems from Stone, Ishii and Bowker, who have prepared BaO particles and films on Pt(111) [19]. The approach may be considered as an inverse model catalyst, with the oxide component supported on an active metallic substrate. The authors were able to follow the growth of Ba, its oxidation to BaO and, finally, the reaction with $NO_2$ by STM. Recently, Bowker, Nix and coworkers presented a comprehensive study of BaO thin films layer growth and reactivity on Cu(111). Ordered BaO layers were prepared [20] and the reaction with $CO_2$, $H_2O$ and $NO_x$ was followed using X-ray photoelectron spectroscopy (XPS), IRAS and thermal desorption spectroscopy (TPD) [21]. The authors were able to show that several reaction steps, including the formation of BaO, hydroxides, carbonates, nitrites and, to some extent, nitrates can indeed be observed in the model approach.

In a second series of model studies, Ozensoy et al. studied the formation of BaO films on $Al_2O_3$/NiAl(100) [22,23] as well as the interaction of $NO_2$ with $Al_2O_3$/NiAl(100) [24,25] and BaO/$Al_2O_3$/NiAl(100) [26] at room temperature. Again the formation of nitrates and nitrites were observed. The nitrate species formed on $Al_2O_3$ were found to be less abundant and less stable than the nitrate species formed on BaO. Upon annealing, a substantial loss of storage capacity was observed, indicating diffusion of BaO into and intermixing with the $Al_2O_3$ support.

One of the most controversially discussed issues is the mechanism of the initial stages of $NO_x$ storage. In several recent studies on model catalysts, it was suggested that the initial product upon interaction of $NO_2$ with the BaO surface are surface nitrites [21, 27,28]. These observations appear to be in agreement with studies on powder catalysts ([7,29], compare also [5]). On the other hand, theoretical calculations by Grönbeck et al. [30,31] and by Schneider and coworkers [32,33] suggest a cooperative adsorption mechanism, involving the formation of nitrite and nitrate pairs.

Addressing this point, Szanyi and coworkers recently performed $NO_2$ adsorption experiments on BaO films on differently prepared $Al_2O_3$ films on NiAl(110) [34,35]. On the basis of IRAS spectra of adsorbed $NO_2$, they concluded that for a thick alumina film (prepared by atomic oxygen treatment of NiAl(110)) there should be strong intermixing of $Ba^{2+}$ and $Al^{3+}$ ions under formation of a barium-aluminate-like phase. In a recent publication we have provided direct evidence for this intermixing process using high-resolution photoelectron spectroscopy (HR-PES) [36]. The formation of such mixed oxides (including aluminate phases) is known from real powder catalysts (see e.g. [5,37]), and may be associated with changes in the storage behavior. In a second set of experiments, Szanyi and coworkers were recently able to provide direct evidence for the simultaneous formation of nitrites and nitrates on a pure BaO film on $Al_2O_3$ at low temperature [35]. Based on this observation the authors suggested that on pure BaO a cooperative adsorption mechanism involving nitrite–nitrate pair formation dominates. The contradictory results in the literature were related to the thin film nature of some model systems and to the formation of barium aluminate phases [35].

In the present paper we address the reaction mechanism on such barium aluminate nanoparticles. The results of a systematic study of the interaction of $NO_2$ with the $Al_2O_3$/NiAl(110) model support and with BaO deposits on $Al_2O_3$/NiAl(110) are presented. The system was previously characterized with respect to its growth behavior and morphology using scanning tunneling microscopy (STM) [38], and with respect to its surface composition using HR-PES [36]. It was shown that upon annealing, thermally stable three-dimensional mixed barium aluminum oxide particles ($BaAl_{2x}O_{1+3x}$) are formed. Here, we probe systematically the reactivity of the model support and the particles as a function of $NO_2$ exposure ($10^{-1}$ to $10^4$ L, 1 L corresponds to $10^{-6}$ Torr s) and surface temperature (100–600 K). Toward this aim, we use time-resolved IR reflection absorption spectroscopy (TR-IRAS) in combination with molecular beam (MB) methods. A complex picture evolves, showing the sequential formation of numerous nitrogen-oxo species, including molecular adsorbates, surface and bulk nitrates and nitrites. In particular, we demonstrate that there is a low-activation-energy cooperative adsorption channel leading to nitrite–nitrate pair formation also on the aluminate particles. However, this reaction channel is restricted to the low temperature regime, suggesting that efficient cooperative adsorption requires molecular adsorption and subsequent $N_2O_4$ dimer formation. If dimer formation is avoided by switching to higher reaction temperatures, the reaction probability drastically decreases and the product spectrum changes to nitrite only. This observation suggests a temperature-dependent change in the reaction mechanism from a cooperative to a non-cooperative pathway. The present findings may help to resolve the contradictory mechanistic picture of the $NO_x$ storage process.

## 2. Experimental

All MB/IRAS (molecular beam/time-resolved IR reflection absorption spectroscopy) experiments were performed in a newly developed UHV (ultrahigh vacuum) apparatus at the University Erlangen-Nuremberg. The setup allows up to four effusive molecular beams and one supersonic molecular beam to be superimposed on the sample surface. Additionally, the system is equipped with a

FTIR spectrometer (Bruker IFS66/v), a beam monitor which allows alignment and intensity calibration of the beams, two quadrupole mass spectrometers (QMS), a vacuum transfer system with high pressure cell and all necessary preparation tools (evaporators, gas doser, quartz microbalance, LEED/Auger, ion gun, etc.). The $NO_2$ beam (Linde, 99.0%) was generated from an effusive beam doser and modulated by a valve system. The backing pressure at the effusive source is typically in the order of 0.1 mbar. At these conditions and 298 K, the fraction of $N_2O_4$ in the gas phase is below 0.1%. All measurements were performed by means of fully remote controlled sequences (interfacing and programming: National Instruments (NI), Lab View, NI). In order to systematically cover a large exposure range, dosing is performed by pulsing $NO_2$ at variable beam intensities typically in the range between $1.6 \times 10^{13}$ $cm^{-2}\,s^{-1}$ (equivalent pressure: $0.7 \times 10^{-7}$ mbar) and $3.2 \times 10^{15}$ $cm^{-2}\,s^{-1}$ (equivalent pressure: $1.4 \times 10^{-5}$ mbar), followed by acquisition of IR spectra (spectral resolution of 2 $cm^{-1}$, typical acquisition times of 38 s). The IR band intensities shown in the following were obtained by integration between the minima after background correction (note that no simple curve fitting procedure can be applied due to exposure-dependent changes in the peak shape, position and width).

For preparation of the model surfaces, a NiAl(110) surface was cleaned by numerous cycles of sputtering and vacuum annealing, followed by two cycles of oxidation in $10^{-6}$ mbar $O_2$ at 550 K and UHV annealing at 1135 K in order to prepare the $Al_2O_3$ film on NiAl(110). With respect to the details of the procedure, we refer to the literature [39–41]. The quality of the film was checked by LEED, and complete oxidation of the surface was proven by the absence of CO adsorption at 100 K.

For the preparation of the BaO particles, we proceeded as follows: First, the Ba metal was manually cleaned under inert gas atmosphere (glove box) and placed into a Mo crucible. In order to prevent oxidation of barium by contact with air, the crucible was filled with decane before being mounted in a commercial electron beam assisted evaporator (Focus EFM3). The evaporator was installed into the UHV chamber immediately before pumping out. Under UHV conditions, the Ba source was calibrated using a quartz microbalance. During deposition the sample was biased to the same potential as the Ba source in order to avoid surface defect generation by Ba ion bombardment. Ba was deposited at 300 K at typical rates of $1.0 \times 10^{13}$ atoms $cm^{-2}\,s^{-1}$ (an average film thickness of 1 Å Ba corresponds to $1.6 \times 10^{14}$ atoms $cm^{-2}$) and subsequently oxidized by exposure to $6 \times 10^{-7}$ mbar $O_2$, for 900 s. In this work we focus on single situation corresponding to a nominal Ba layer thickness of 20 Å. This corresponds to a Ba atom density of $3.2 \times 10^{15}$ atoms $cm^{-2}$.

## 3. Results and discussion

### 3.1. Structural and chemical characterization of the model $NO_x$ storage material

In a first step we briefly summarize previous results on the nucleation and growth behavior of the BaO nanoparticles on NiAl(110) and on the chemical properties of the particle surface. For more details, we refer to the literature [36,38].

Selected STM images are displayed in Fig. 1 (see also [38]). As a model support, we utilize an ordered, atomically flat $Al_2O_3$ film, prepared on NiAl(110) [40,42]. This film has been characterized in detail with respect to its structure and adsorption properties. Recently, its microscopic structure has been solved by STM in combination with DFT (density function theory) calculations [41]. Also, the film has been used as a model support for metal nanoparticles in several cases (see e.g. [13,15,43]). Fig. 1a shows the typical defect structure of the film (compare [44]). In addition to the steps,

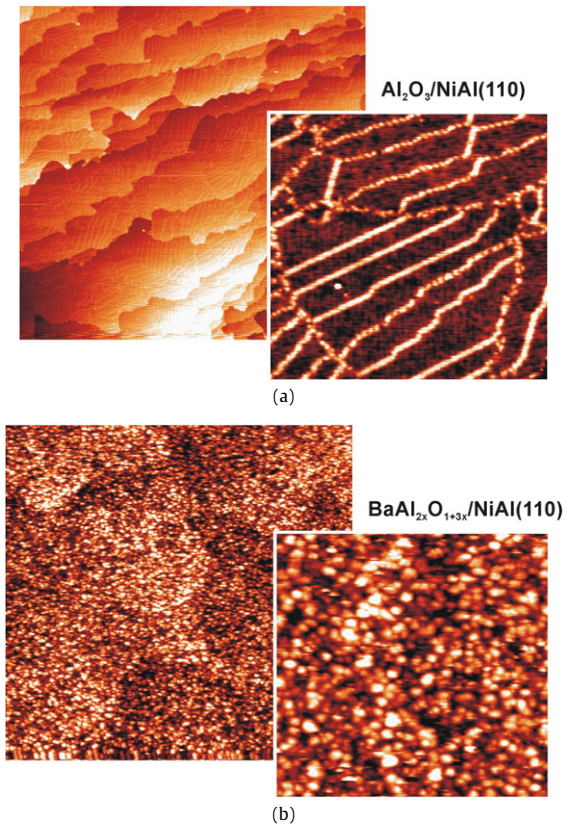


**Fig. 1.** (a) STM images of the pristine $Al_2O_3$/NiAl(110): overview (800 nm × 800 nm, CCT (constant current topography), $I = 0.194$ nA, $U = 3.5$ V) and close-up (100 nm × 100 nm, CCT, $I = 0.150$ nA, $U = 3.0$ V). (b) STM image of the $BaAl_{2x}O_{1+3x}$ nanoparticles on $Al_2O_3$/NiAl(110), prepared by deposition of 20 Å Ba and subsequent oxidation and annealing, overview (500 nm × 500 nm, CCT, $I = 0.183$ nA, $U = 2.0$ V) and close-up (100 nm × 100 nm, CCT, $I = 0.183$ nA, $U = 2.6$ V); see also [38].

originating from the NiAl(110) support, we observe a characteristic network of domain boundaries (primarily antiphase domain boundaries, visible as line protrusions in Fig. 1a). Onto this film, Ba metal is deposited at a surface temperature of 300 K, followed by extended exposure to oxygen ($1 \times 10^{-6}$ mbar, 900 s). Subsequently, the surface is annealed to 800 K in oxygen ($1 \times 10^{-6}$ mbar) in order to stabilize the particles and to decompose $BaO_2$ species, which may be formed at room temperature (compare [23]).

Next, the supported BaO nanoparticles system can be characterized by STM. Corresponding images are displayed in Fig. 1b. In a previous study it was shown that starting from low coverage, the formation of three-dimensional nanoparticles is observed, which nucleate both at the $Al_2O_3$ domain boundaries and on the domains [38]. From STM, we derive a particle density of $(5.6 \pm 1.0) \times 10^{12}$ $cm^{-2}$ at a nominal Ba layer thickness of 20 Å Ba ($3.2 \times 10^{15}$ Ba atoms $cm^{-2}$). This corresponds to nanoparticles containing $(560 \pm 100)$ $Ba^{2+}$ ions in average. In comparison with the growth of other metals on the same support, the nucleation density for Ba at 300 K is rather high, indicating a strong interaction of Ba with the support and a short diffusion length (see e.g. [43]). This hypothesis is supported by the STM experiments which suggest the formation of flat islands with aspect ratios around 1:5 (height:diameter). Here, it should be noted, however, that the exact aspect ratio is difficult to extract from STM due to the different electronic structure of the BaO and the support and due to convolution with the tip shape.

In a second study, we have investigated the electronic structure and chemical composition of the model system by HR-PES using synchrotron radiation [36]. The most important result from

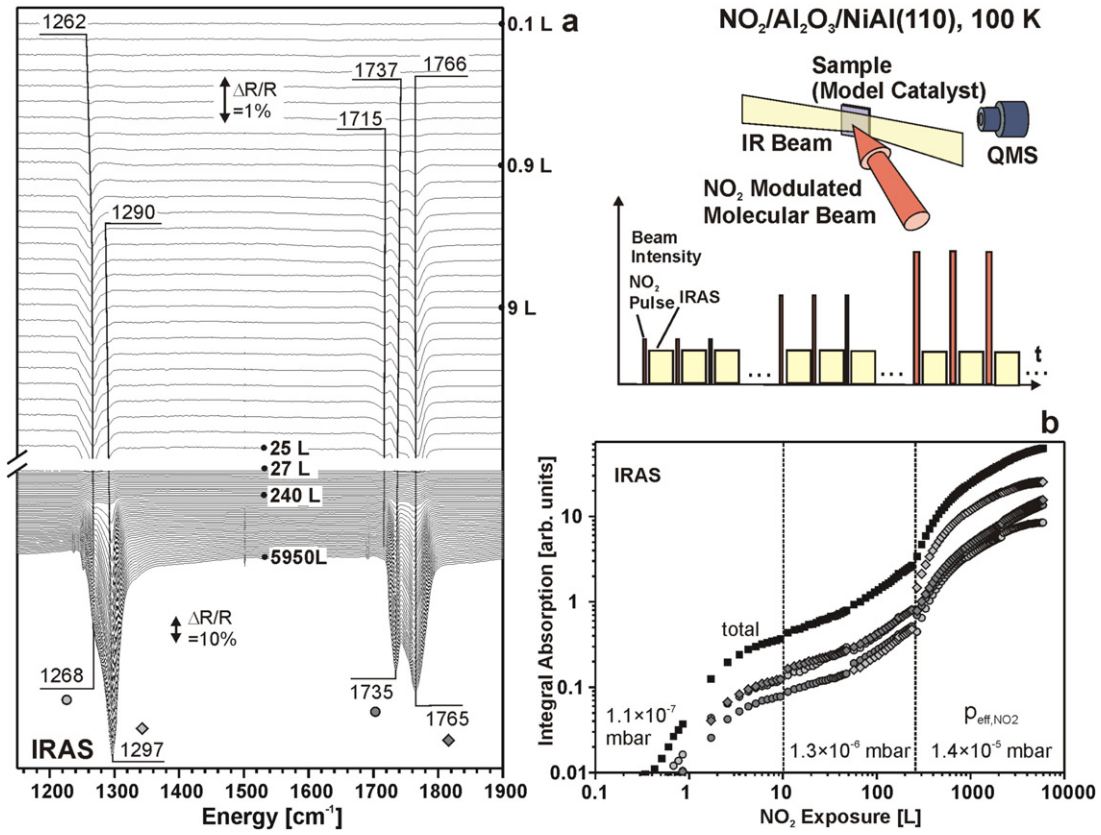


**Fig. 2.** Interaction of $NO_2$ with the pristine $Al_2O_3$/NiAl(110) at 100 K: (Top right) Experimental setup and the experimental procedure (see text for details); (a) IR reflection absorption spectra of the NO stretching frequency region as a function of $NO_2$ exposure; (b) integral absorption of the most prominent spectral features and total absorption in the NO stretching frequency region as a function of $NO_2$ exposure. Note that the effective $NO_2$ pressure during the $NO_2$ pulses was varied between the experiments. The corresponding values are given in the figure.

this study was that upon Ba deposition and $O_2$ exposure, strong intermixing of $Ba^{2+}$ and $Al^{3+}$ ions occurs, even at 300 K. Upon annealing to 800 K in $O_2$, the support oxide film grows in thickness and complete intermixing of $Ba^{2+}$ and $Al^{3+}$ ions occurs, leading to the formation of barium aluminate like particles (in the following denoted as $BaAl_{2x}O_{1+3x}$). These particles represent a thermally very stable model system and show typical $NO_x$ storage and release properties of Ba-based $NO_x$ storage materials [38].

In the following we investigate the reaction of $NO_2$ with this model surface. In a first step we focus on the reaction of $NO_2$ with the pure $Al_2O_3$ support (Section 3.2), before in the next section we proceed to the interaction of $NO_2$ with the supported $BaAl_{2x}O_{1+3x}$ nanoparticles (Sections 3.3 and 3.4).

### 3.2. Adsorption and reaction of $NO_2$ on $Al_2O_3$/NiAl(110)

In order to systematically probe the interaction of $NO_2$ with the model surfaces, we acquire series of IRAS spectra taken in a fully remote-controlled sequence in combination with MB dosing. The schematic setup and procedure is shown in the inset of Fig. 2a. Pulses of $NO_2$ of different duration and intensity are applied, with each pulse followed by acquisition of an IR spectrum. The $NO_2$ dose is automatically varied between approximately 0.1 and 130 L per pulse (1 L corresponds to $10^{-6}$ Torr s), allowing us to cover an exposure range between approximately 0.1 and 6000 L in a single experiment. To start with, we probe the adsorption of $NO_2$ on the pristine $Al_2O_3$/NiAl(110) film at 100 K. The corresponding IR spectra are displayed in Fig. 2a. Fig. 2b shows the integral intensity of the different spectral features in the NO stretching frequency region as well as the total integral intensity as a function of exposure.

At low exposure (<1 L), we initially observe bands at 1262 and 1766 $cm^{-1}$ together with weaker absorption features at 1737 and 1715 $cm^{-1}$. With increasing exposure, all bands grow in intensity. At exposures above 10 L, the band at 1715 $cm^{-1}$ saturates whereas the other features continue to grow. Simultaneously, a fifth band appears at 1290 $cm^{-1}$, which blue-shifts to 1297 $cm^{-1}$ and, finally, becomes the dominant feature in the high coverage region. The bands at 1262 $cm^{-1}$ blue-shifts to 1268 $cm^{-1}$ and in the high coverage region is only visible as a shoulder of the band at 1297 $cm^{-1}$.

$NO_2$ adsorption at low temperature has been studied by IR spectroscopy on various substrates (see e.g. [45–48]) including a recent study by Ozensoy et al. on an ordered alumina film on a similar substrate ($Al_2O_3$/NiAl(100) [25]). In accordance with this work, the regions around 1250 to 1300 $cm^{-1}$ can be assigned to the ONO symmetric stretching mode ($\nu_s$(ONO)) and the region around 1750 $cm^{-1}$ to the antisymmetric mode ($\nu_{as}$(ONO)) of the $N_2O_4$ dimer with $D_{2h}$ symmetry. No indications for detectable concentrations of other species, especially the asymmetric isomer (ONO–$NO_2$), nitrosonium nitrate ($NO^+NO_3^-$) or monomeric $NO_2$ derived species are observed [49]. The splitting of bands in both the $\nu_{as}$(ONO) and the $\nu_s$(ONO) region has been observed in previous studies as well, and has mainly been attributed to surface and bulk layers of $N_2O_4$ [25,45,48]. Other potential origins of band shifts, splitting or broadening effects are possible ordering processes within the $N_2O_4$ layers and interaction with coadsorbates such as e.g. $H_2O$. Closely inspecting the data shown in Fig. 2a, it is found that the coverage dependence of the features at 1268 and 1715 $cm^{-1}$ indeed shows a saturation behavior, which would be compatible with the assignment to a surface or monolayer species. However, the peak at 1735 $cm^{-1}$, which was previously attributed to the monolayer, continues to grow while retaining a constant in-

tensity ratio with respect to the bulk feature at 1765 $cm^{-1}$. Therefore, we propose to assign both bands, 1735 and 1765 $cm^{-1}$, to the $N_2O_4$ multilayer. The origin of the splitting is not clear, but may be due to intermolecular vibrational coupling or interactions in the bulk layer.

The two bands at 1268 and 1715 $cm^{-1}$ are assigned to the $N_2O_4$ monolayer. It is apparent that the intensity ratio $I(\nu_{as})/I(\nu_s)$ is dissimilar for the monolayer and the bulk features. Taking into account the polarization of modes ($\nu_{as}$(ONO): polarized perpendicular to N–N axis; $\nu_s$(ONO): polarized parallel to N–N axis) and the MSSR (metal surface selection rule) [50], this intensity ratio provides information on the average orientation of the $N_2O_4$ molecules with respect to the surface normal (compare e.g. [48]). For the monolayer peaks, the symmetric mode is dominant, indicating preferential orientation of the $N_2O_4$ molecule with the N–N axis perpendicular to the surface. In contrast, the multilayer shows a different behavior. At lower coverage (exposure <100 L) the asymmetric modes (1735 and 1765 $cm^{-1}$) dominate, pointing to an N–N axis preferentially oriented parallel to the surface. With increasing coverage, the intensity of both regions becomes comparable (similar as in the gas phase) indicating that the preferential orientation is successively lost and a rather randomly oriented layer is obtained.

It is important to note that adsorption of $NO_2$ is purely molecular on $Al_2O_3$/NiAl(110) at 100 K and there is no indication for the formation of surface nitrites or nitrates. In order to test the reactivity of the model support at higher temperatures, we perform a similar experiment at a surface temperature of 300 K. The experimental procedure is equivalent to the one described above for adsorption and reaction at 100 K. The corresponding spectra are displayed in Fig. 3a. Fig. 3b shows the integral intensity of the features in the NO stretching frequency region as well as the intensity of some individual bands marked in the spectra.

The behavior is very different from the experiment at 100 K. We observe very slow formation of weak bands at exposures larger than approximately 100 L, initially in the regions from 1200 to 1250 $cm^{-1}$ and around 1600 $cm^{-1}$. At exposures larger than 2000 L four distinct bands appear at 1255, 1297, 1595 and 1652 $cm^{-1}$. Here, the two bands at high frequency dominate. Focusing on these two high frequency bands, it is observed that their relative intensity undergoes drastic changes as a function of $NO_2$ exposure. Whereas the band at 1595 $cm^{-1}$ dominates at low exposure, the feature at 1652 $cm^{-1}$ rapidly grows in intensity at exposures exceeding approximately 2000 L (see inset in Fig. 3b). At the highest exposures applied in this study (approximately 6000 L), the band at 1652 $cm^{-1}$ represents the dominating one in this region.

The interaction of $NO_2$ with $Al_2O_3$ at room temperature and above has been studied both on $Al_2O_3$ powders (see e.g. [51,52], also [53]) and, recently, on $Al_2O_3$ thin films [24]. The assignments have been discussed and used by several authors in studies on alumina-supported NSR catalysts [7,52–56]. With respect to a detailed discussion on the identification of nitrogen-oxo species by means of vibrational spectroscopy we refer to a recent review by Hadjiivanov [49].

On the basis of the above mentioned studies, we derive the following assignment. Goodman et al. [51] investigated the interaction of alumina powders with $NO_2$ as a function of pressure. Initially, they observed absorption features around 1230 $cm^{-1}$ (and a weak band at 1312 $cm^{-1}$), which they assigned to a nitrito species. This interpretation would be compatible with a recent XPS study by Ozensoy et al. [24], showing that at low temperature nitrites are formed upon exposure of an ordered $Al_2O_3$ film to $NO_2$. Thus we attribute the initial appearance of weak absorption bands in the region around 1200 to 1250 $cm^{-1}$ to the formation of $NO_2^-$ surface species. This assignment is confirmed by a recent HR-PES study on the same model system [36].

The four bands appearing at higher exposure can be attributed to surface nitrates. The formation of nitrates on $Al_2O_3$ was experimentally observed by numerous groups [51,54–56]. Upon adsorption on a surface, the two-fold degenerate asymmetric stretching mode $\nu_3$ of ionic $NO_3^-$ (1380 $cm^{-1}$) splits into two bands (see [51], compare also [49,57]). The exact position and splitting depends on the adsorption site and geometry. Typically, the splitting is assumed to be larger for bridging nitrates and smaller for chelating and monodentate nitrates [49,51,54–56]. Goodman et al. [51] observed bands at 1622/1260 $cm^{-1}$, 1587/1292 $cm^{-1}$, 1555/1308 $cm^{-1}$, which they attributed to bridging, chelating and monodentate nitrate, respectively. A similar assignment was given by Westerberg and Fridell [54] who observed the corresponding features at 1630 and 1266 $cm^{-1}$ (bridging nitrate), 1612 and 1293 $cm^{-1}$ (chelating nitrate) and 1588 and 1297 $cm^{-1}$ (monodentate nitrate) in the limit of high coverage. In a similar study on powder NSR catalysts, Sedlmair et al. [56] assigned features at 1620 and 1260 $cm^{-1}$ to the bridging nitrate and 1560 and 1290 $cm^{-1}$ to the bidentate chelate. Slightly different frequency ranges were suggested by Prinetto et al. [55] (monodentate: 1420–1500 $cm^{-1}$, 1300–1400 $cm^{-1}$; bidentate chelate: 1570 $cm^{-1}$, 1290 $cm^{-1}$; bridging bidentate: 1240–1250 $cm^{-1}$, 1590–1600 $cm^{-1}$).

Based in these assignments, one could tentatively attribute the bands at 1255 and 1652 $cm^{-1}$ to a bridging nitrate, whereas the bands at 1297 and 1595 $cm^{-1}$ may be assigned to a monodentate or chelating bidentate. It should be noted, however, that these "traditional assignments" of the vibrational bands mainly rely on comparisons with transition metal complexes (see e.g. [49,57] and references therein), and such comparisons have failed for surface species in several cases (compare e.g. [58]). As there are hardly any independent experimental evidences for the adsorption geometry and coordination of the respective species, the corresponding assignments should, therefore, be treated with utmost care.

Toward an unambiguous identification of adsorption geometries, we have recently shown that valuable information on the coordination of nitrates on planar metal supported model surfaces can not only be extracted from the band positions but also from their relative intensities [59]. In contrast to the powder spectra exhibiting similar band intensities in both frequency regions, for the surface nitrates observed on $Al_2O_3$/NiAl(110) the high frequency region strongly dominates (see Fig. 3b). This observation can be straightforwardly explained on the basis of the MSSR, assuming a bridging coordination and a binding geometry nearly perpendicular to the surface plane. In case of the bridging nitrate, the high-frequency component of $\nu_3$ is polarized perpendicular to the surface plane, whereas the low-frequency mode shows nearly parallel polarization and, consequently, should be largely screened by the metal surface. For a monodentate nitrate the situation would be vice versa, with the high-frequency mode showing parallel and the low-frequency mode showing perpendicular polarization (see [59] for details). Following these arguments, monodentate coordination can be excluded, and both features are assigned to a bridging or chelating-bidentate. The frequency shift may be due to different coordination geometry and/or due to different adsorption sites. We will discuss the identification of differently coordinated nitrate species in more detail in connection with the surface nitrates on BaO (see Section 3.3).

Finally, it should be noted that the coverage-dependent development of the intensities of the individual bands (Fig. 3b) reveals a sequential formation of both surface nitrate species. Initially the species is formed, which gives rise to the two lower frequency bands (1255 and 1595 $cm^{-1}$). A possible assignment would be related to nitrate formation at oxide defects such as e.g. antiphase

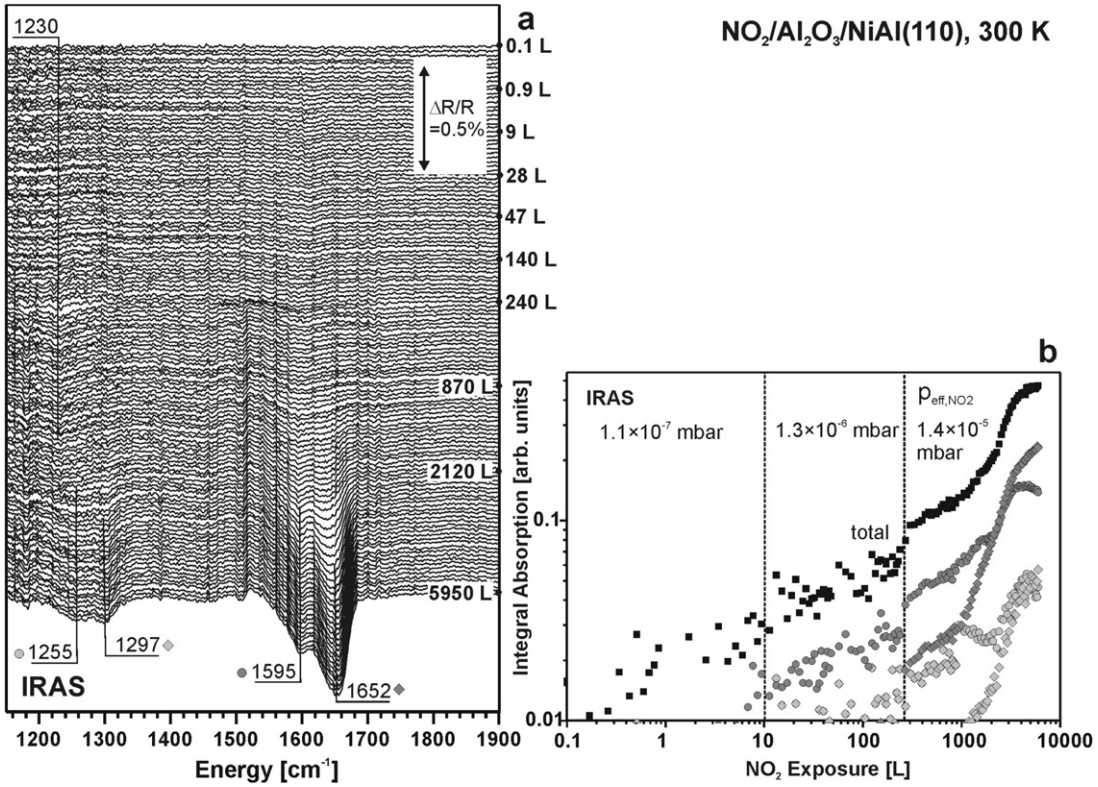


**Fig. 3.** Interaction of $NO_2$ with the pristine $Al_2O_3$/NiAl(110) at 300 K: (a) IR reflection absorption spectra of the NO stretching frequency region as a function of $NO_2$ exposure; (b) integral absorption of the most prominent spectral features (gray symbols) and total absorption (black symbols) in the N–O stretching frequency region as a function of $NO_2$ exposure.

domain boundaries [40,44]. Exceeding exposures of approximately 1000 L, however, the intensity of the high frequency components (1297 and 1652 $cm^{-1}$) increases dramatically, finally dominating the vibrational spectrum. Discussing the intensity of IRAS bands it should be noted that these may show a strongly nonlinear coverage dependence due to dipole coupling effects [50]. Still, the observation suggests that the initial reaction of $NO_2$ takes place at defects of the $Al_2O_3$ film, finally followed by structural transformations of the film, which facilitate bonding of nitrates on the domain terrace sites themselves.

### 3.3. Reaction of $NO_2$ with $BaAl_{2x}O_{1+3x}$ nanoparticles between 100 and 300 K

After analysis of the reaction of $NO_2$ with $Al_2O_3$, we now focus on the interaction with the supported $BaAl_{2x}O_{1+3x}$ nanoparticles. In a first step, we probe the reaction at 300 K. The corresponding IRAS data is displayed in Fig. 4. The experimental procedure applied corresponds to the experiments performed on the pristine $Al_2O_3$ film. Again, Fig. 4b shows the integral intensity in the region of the NO stretching modes and the individual intensity of selected bands as a function of $NO_2$ exposure.

Close inspection of the spectra at low exposure reveals that very weak features initially emerge between 10 and 1000 L in the region around 1230–1250 $cm^{-1}$. Later, bands at 1326 to 1334 $cm^{-1}$ and around 1465 $cm^{-1}$ appear. The band at 1465 $cm^{-1}$ grows more rapidly than the lower-frequency peaks and becomes dominant for exposures larger than 3000 L. Considering the band intensity as a function of $NO_2$ exposure (Fig. 4b), a pronounced nonlinear behavior with $NO_2$ exposure is observed. Whereas in the low exposure regime the bands grow only slowly, their intensity starts to increase rapidly at exposures exceeding approximately 1000 L, before finally saturating above 4000 L.

The interaction of $NO_2$ with BaO near room temperature has been studied by several groups, with observations and spectral assignments differing to some extent [7,21,29,52–56,60–62]. Prinetto et al. also assigned bands at 1220 and 1330 $cm^{-1}$ to bidentate and ionic nitrites [55]. On the basis of theoretical calculations, Broqvist et al. came to a similar conclusion (for bands 1250 and 1330 $cm^{-1}$) [62], however, they questioned previous assignments of the peaks at 1420 and 1475 $cm^{-1}$ to linear nitrites [62]. In contrast, Hess and Lunsford attributed bands at 1225 and 1327 $cm^{-1}$ to N-coordinated nitrite (nitro species) and ionic nitrites [29,61]. Sedlmair et al. investigated the reaction of $NO_2$ with a commercial NSR catalyst (containing also Pt) at 323 K [56]. At low exposure they observed bands at 1203, ~1330 and 1419 $cm^{-1}$, which they attributed to bidentate nitrites ("bridging bidentate nitrito species," compare [49]) ($\nu_s$(ONO) and $\nu_{as}$(ONO)) and linear nitrites ("linear nitrito species," compare [49]) respectively. The nitrite bands around 1200 $cm^{-1}$ were observed to decrease with increasing exposure, while new bands at 1429 $cm^{-1}$ and above appeared. The bands at 1429 and 1332 $cm^{-1}$ were attributed to monodentate nitrates, whereas all bands above 1500 $cm^{-1}$ were assigned to nitrate species on $Al_2O_3$ [56]. Other reported frequencies for the monodentate nitrate species are at 1291 and 1542 $cm^{-1}$ (by Westerberg and Fridell [54]). For bidentate nitrates on $BaO/Al_2O_3$, frequencies of 1214 and 1573 $cm^{-1}$ were reported by Westerberg and Fridell [54] and frequencies of 1200–1320 $cm^{-1}$ and 1540–1650 $cm^{-1}$ by Prinetto et al. [55]. These species, however, may at least partially be located on or in the vicinity of alumina support sites.

The interaction of BaO films with $NO_2$ under UHV condition was recently studied by Tsami et al. [21]. In this study, the authors investigated the reaction of $NO_2$ with an ordered BaO thin film on Cu(111), applying XPS (X-ray photoelectron spectroscopy), TPD (thermal desorption spectroscopy) and IRAS [21]. In agreement with the above interpretation, the formation of nitrites was

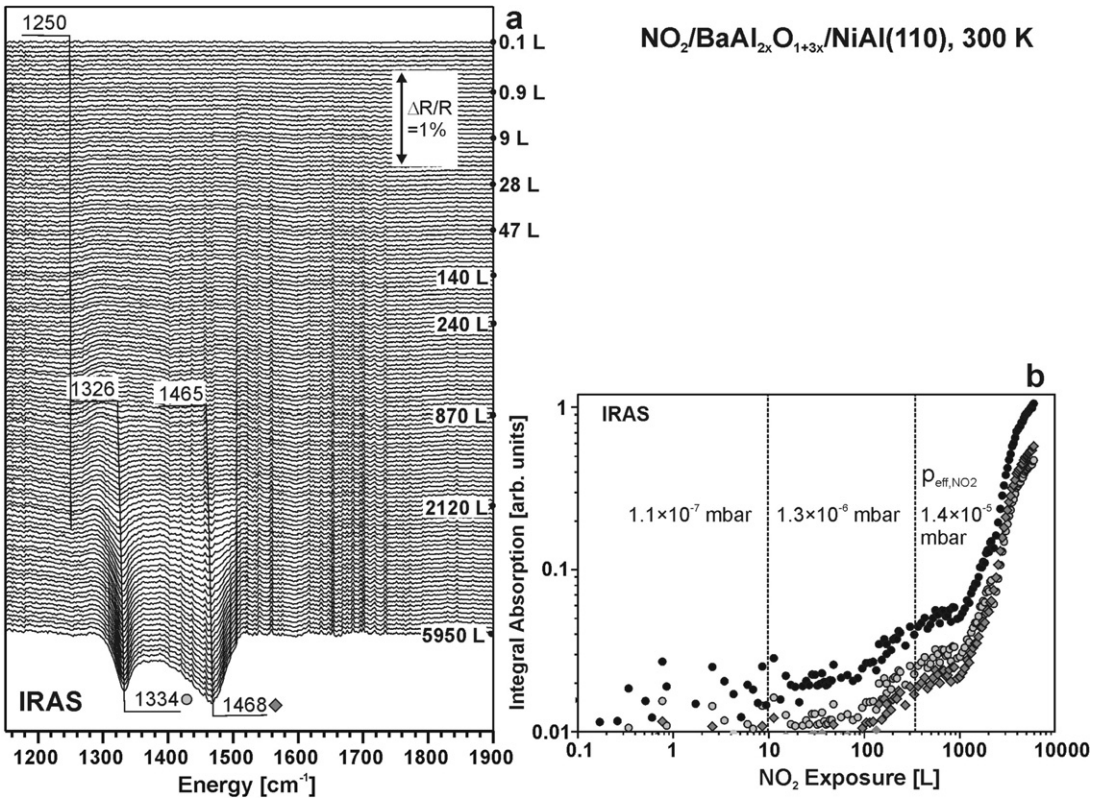


**Fig. 4.** Interaction of $NO_2$ with the $BaAl_{2x}O_{1+3x}$ nanoparticles supported on $Al_2O_3$/NiAl(110) at 300 K: (a) IR reflection absorption spectra of the NO stretching frequency region as a function of $NO_2$ exposure; (b) integral absorption of the most prominent spectral features (gray symbols) and total absorption in the N–O stretching frequency region (black symbols) as a function of $NO_2$ exposure.

observed at the initial stage of the reaction, which, subsequently, were transformed into nitrates at higher exposure. Szanyi and coworkers argued that the initial formation of nitrites may be due to the thin film nature of these model surfaces or due to the formation of aluminate-like phases [35].

Motivated by this somewhat unclear situation, we have recently carried out a correlated XPS/IRAS study, in order to quantify the amount of nitrite and nitrate formation and identify the vibrational spectra of the corresponding species [28]. The following conclusion could be derived: For reaction at 300 K, XPS shows exclusively the formation of barium nitrites during the initial stages of $NO_2$ exposure. The corresponding IRAS spectra are characterized by a weak and broad band around 1230–1250 $cm^{-1}$. In connection with density functional theory (DFT) calculations by Grönbeck et al. (see [30,59]), the very low intensities of the nitrite bands were attributed to a bonding geometry, with the $NO_2^-$ ion lying nearly flat on the surface (i.e. nitrito or nitro-nitrito coordination, see [59]; the low intensity is a consequence of the MSSR). The appearance of the band at 1330 $cm^{-1}$ was found to be not correlated to the formation of any new nitrite species [28]. Therefore, the bands at 1330 and 1465 $cm^{-1}$ can be assigned to the two components of the split $\nu_{as}(NO_3^-)$ mode of surface nitrates, exclusively.

The question arises, whether the coordination geometry of surface nitrates on BaO (monodentate or bridging) can be identified on the basis of vibrational spectroscopy. Based on a combined DFT/IRAS study, we have recently argued that this may not be possible solely on the basis of the position of the vibrational bands [59]. As discussed in Section 3.2, however, valuable information on the bonding geometry is available from the relative band intensities of the two components of $\nu_{as}(NO_3^-)$ [59]. Again, the low frequency component of $\nu_{as}(NO_3^-)$ should be polarized perpendicular to the surface in case of the monodentate and, as a consequence of the MSSR, the band around 1300 $cm^{-1}$ is expected to dominate the spectrum. The situation is reversed for the bidentate, for which the high frequency (~1460 $cm^{-1}$) component shows perpendicular polarization. Following these arguments, the behavior of the relative intensities would indeed suggest initial formation of monodentate nitrates, whereas at high exposures the bidentate species dominates. To some extent, the latter conclusion contrasts the "traditional" assignment of bands in this frequency region to predominately monodentates (see e.g. [7,21,29,52–56,60–62], compare discussion in [59]). It should be pointed out, however, that other aspects such as dipole coupling and intensity transfer effects [50,63] or the morphology of the BaO particles require more thorough consideration at this point, and, accordingly, we restrict ourselves to qualitative considerations and refer to the literature for a detailed discussion ([59], see e.g. [28] for a comparison of quantitative XPS data and IRAS).

It is noteworthy, that the intensity of the nitrate related bands shows a strongly nonlinear behavior as a function of $NO_2$ exposure. Similar as in the case of the pristine $Al_2O_3$, we may assume that the initial reaction gives rise to structural transformations of the BaO particle surface, leading to enhanced reactivity after an initial induction period. It is noteworthy that, in spite of the high surface concentration of $Al^{3+}$ ions on the $BaAl_{2x}O_{1+3x}$ nanoparticles (see [36]), there are no indications for the characteristic surface nitrate bands on $Al_2O_3$ (see Section 3.2). This observation may suggest that, upon reaction with the $BaAl_{2x}O_{1+3x}$ particles, the surface nitrates formed predominately interact with $Ba^{2+}$ ions. This hypothesis would be in line with an observation by Szanyi and coworkers [34], who suggested that the reaction of a Ba-aluminate-like layer with $NO_2$ leads to removal of $Ba^{2+}$ ions from the mixed oxide phase and formation of $Ba(NO_3)_2$.

As outlined in the introduction, the present observation of only nitrites being formed during the initial stage of the reaction may appear to be in contrast with recent results by Szanyi and

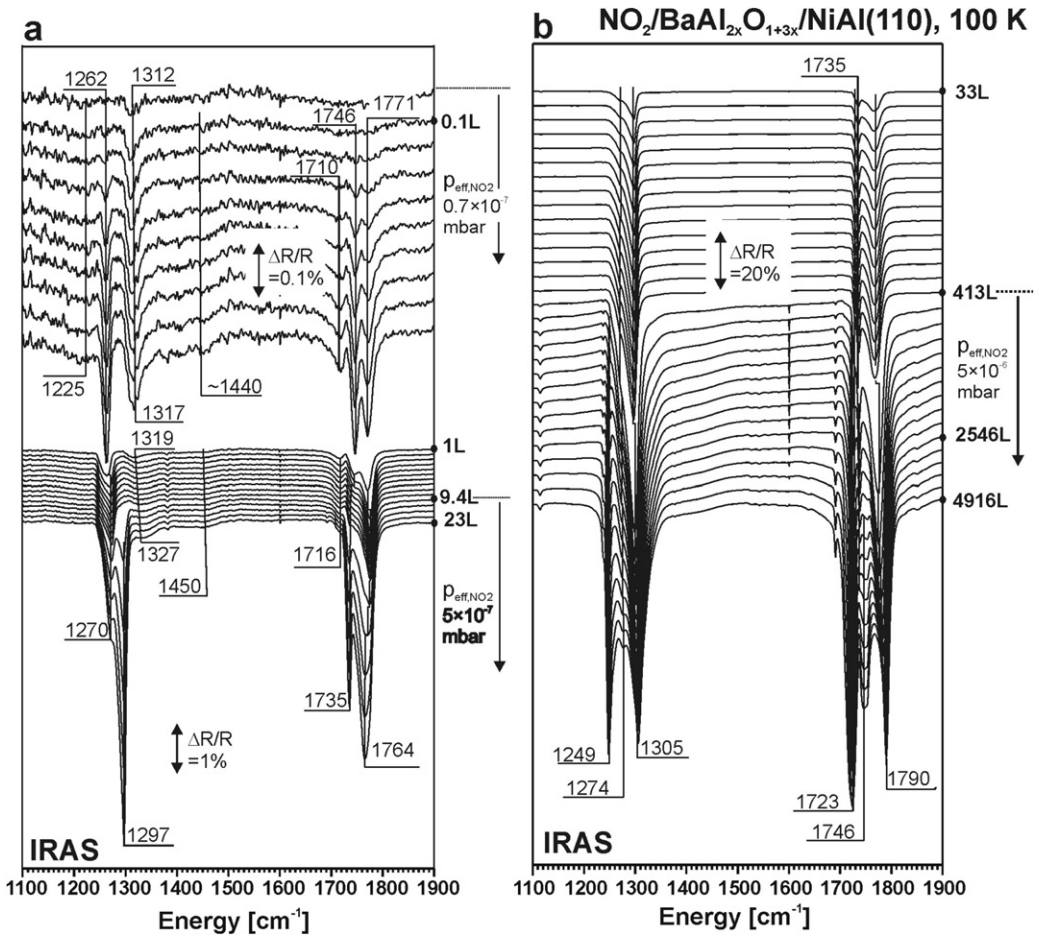


**Fig. 5.** Interaction of $NO_2$ with the $BaAl_{2x}O_{1+3x}$ nanoparticles supported on $Al_2O_3$/NiAl(110) at 100 K: IR reflection absorption spectra of the NO stretching frequency region as a function of $NO_2$ exposure in the region of low $NO_2$ exposures (a) and high $NO_2$ exposures (b).

coworker [34]. By means of XPS and IRAS experiments on a BaO film, they were able to provide direct evidence for the simultaneous formation of nitrates and nitrites. These results provide direct evidence for the existence of a cooperative reaction mechanism. It should be pointed out that these experiments were carried out on BaO thin films, which were prepared via a special procedure aiming at the formation of a pure BaO films with a minimum of intermixing with the $Al_2O_3$ support. The authors concluded that the contradictory results in the literature may be the result of the specific properties of thin film model systems and, in particular, the result of the formation of Ba-aluminate phases which can be formed if the BaO is deposited on an $Al_2O_3$ support.

It is noteworthy that the experiments by Szanyi et al. were performed at low temperatures in the presence of molecularly adsorbed $N_2O_4$. In order to test, whether Ba aluminate formation indeed gives rise to a change in reaction mechanism, we have probed the reaction of $NO_2$ with the $BaAl_{2x}O_{1+3x}$ nanoparticles at low temperatures as well. The corresponding spectra for an experiment performed at a surface temperature of 100 K are displayed in Fig. 5.

Starting from the lowest exposures (0.05 L), we observed a distinct band emerging at 1312 $cm^{-1}$. In the exposure region between 0 and 1 L, this band slowly increases in intensity and shifts to 1320 $cm^{-1}$. Simultaneously, two weak and broad features appear around 1230 $cm^{-1}$ and around 1440 $cm^{-1}$. In addition, several sharp bands appear around 1260, 1710, 1740 and 1770 $cm^{-1}$. At larger exposures, the latter bands develop into several intense and sharp bands between 1250 and 1300 $cm^{-1}$ and between 1720 and 1790 $cm^{-1}$, which continuously grow in intensity with increasing exposure.

Based on the discussion in Section 3.2, the sharp bands in the region between 1250 and 1300 $cm^{-1}$ can be attributed to the ONO symmetric stretching mode ($\nu_s$(ONO)) of the $N_2O_4$ dimer and the bands in the region around 1750 $cm^{-1}$ to the antisymmetric mode ($\nu_{as}$(ONO)) of $N_2O_4$. Thus, we conclude that at large exposures there is mainly molecular adsorption of $NO_2$ in the form of the $D_{2h}$ dimer, similar as was observed on the pristine $Al_2O_3$ support.

Of particular interest is the region of low $NO_2$ exposures. The bands around 1230, 1320 and 1440 $cm^{-1}$ are not observed on the Ba-free model support (compare Fig. 2) and, therefore, cannot be attributed to molecular $N_2O_4$. Based on the above discussion, we attributed the band at 1230 $cm^{-1}$ to surface nitrites and bands at 1320 and 1440 $cm^{-1}$ to surface nitrates. This assignment is in full agreement with the work by Szanyi and coworkers, who reported bands at 1225, 1342 and 1429 $cm^{-1}$ [34]. Taking into account the intensity ratio between the two components of $\nu_{as}(NO_3^-)$, we identify the nitrate as a monodentate species (compare discussion above and [59]).

The most important conclusion from the present experiment is that at 100 K we observe simultaneous formation of both nitrites and nitrates on the mixed $BaAl_{2x}O_{1+3x}$ nanoparticles. This observation is in sharp contrast to the behavior at 300 K (see Fig. 4). It confirms the existence of a cooperative adsorption mechanism, leading to nitrite–nitrate pair formation also in the case of mixed barium aluminum oxide particles.

In order to identify the origin of the temperature-dependent changes in the reaction behavior, it is helpful to directly compare

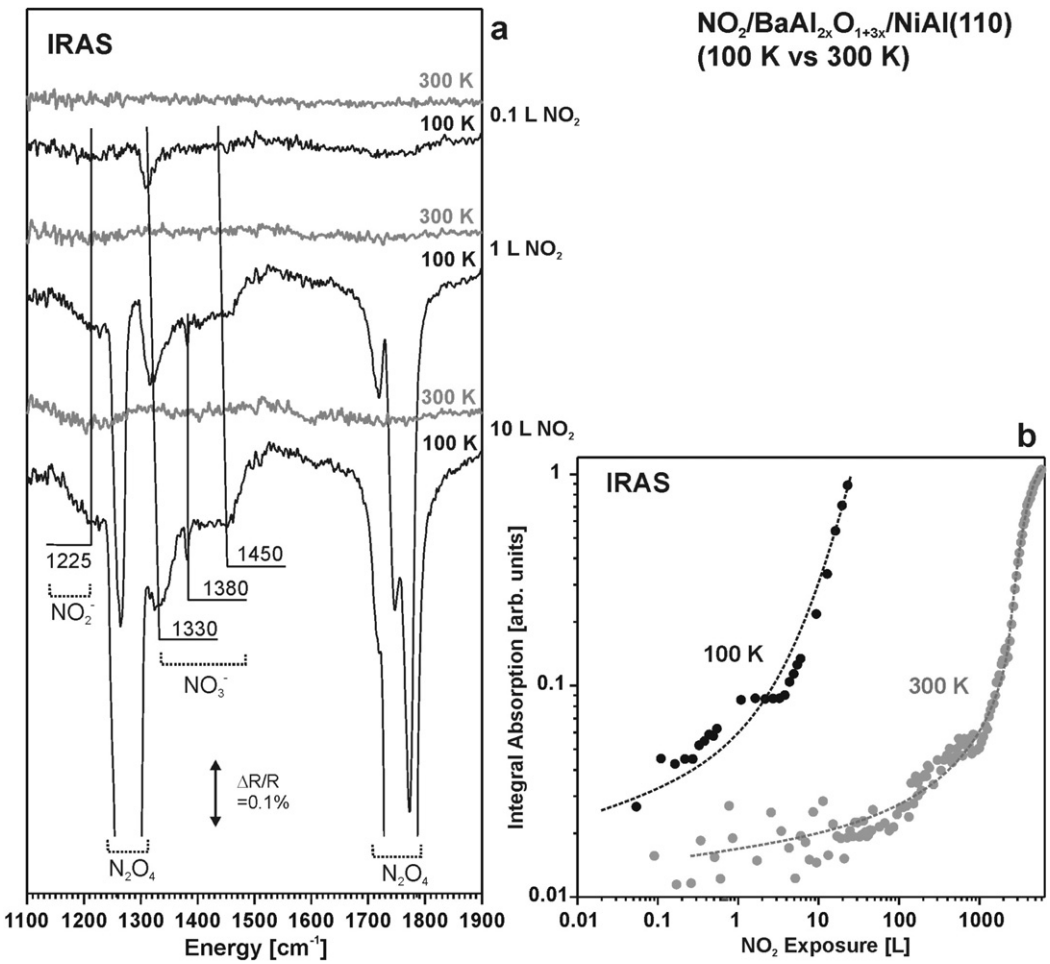


**Fig. 6.** Comparison of IR reflection absorption spectra obtained during reaction of the $BaAl_{2x}O_{1+3x}$ nanoparticles supported on $Al_2O_3$/NiAl(110) at 100 K (black lines) and at 300 K (gray lines); (b) integral absorption in the region of the nitrate related bands between 1300 and 1550 $cm^{-1}$ as a function of $NO_2$ exposure during reaction at 100 K (black symbols) and at 300 K (gray symbols).

the IRAS spectra obtained for reaction at 100 and at 300 K. A corresponding plot is displayed in Fig. 6a. It is apparent that for reaction at 100 K the characteristic nitrate bands already appear at the very lowest exposures (0.05 L). This behavior suggests a very high reaction probability and a low activation barrier. It is noteworthy, that the nitrate (and nitrite) bands appear even before there is any indication of molecularly adsorbed $N_2O_4$. Only after formation of some initial amount of nitrates and nitrites, molecularly adsorbed $N_2O_4$ is accumulated. If we increase the reaction temperature to 300 K, we find three major differences. First, there is no molecular adsorption of $N_2O_4$ at this temperature. Secondly, the initial product spectrum changes to the formation of nitrites only. The third point is related to the reaction probability, which is decreasing significantly. A comparison of the integral intensities of the IR bands in the nitrate region is displayed in Fig. 6b. It is apparent that at 300 K the formation of nitrates occurs at a rate, which is by a factor of $10^2$ to $10^3$ lower than compared to 100 K.

From the above discussion, we may draw the following conclusions. Apparently, it is not the formation of mixed barium aluminum oxides, which controls the reaction mechanism. Instead, the most critical factor appears to be the reaction temperature. At low reaction temperatures, a highly efficient reaction channel with low activation energy leads to the formation of nitrite–nitrate pairs. It is noteworthy, that the temperature region in which this mechanism dominates coincides with the region of molecular adsorption of $NO_2$. As molecular adsorption occurs under dimerization, we tentatively associate the low temperature cooperative adsorption mechanism to the presence of $N_2O_4$ dimers on the surface. Besides the traditional pathway in which the individual $NO_2$ fragments directly interact with the surface, followed by an electron transfer process (compare [30–32,64]), the dimerization-mediated pathway may involve disproportionation via isomerization to asymmetric dimer (ONO–$NO_2$), possibly followed by formation of nitrosonium nitrate ($NO^+NO_3^-$). The resulting Lewis acid/base pair may directly react with suitable Lewis base/acid sites on the Ba aluminate particles:

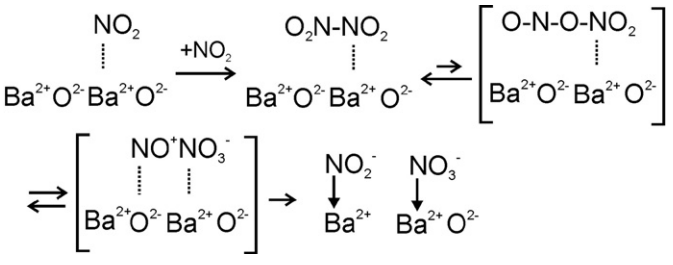


(1)

Isomerization between the two $N_2O_4$ dimers is facile (see [65] and references therein). It may occur easily, even at low temperature, via dissociation of the N–N bond and subsequent recombination (the dissociation energy for the $N_2O_4$ dimer is 57 kJ $mol^{-1}$ in the gas phase and may be further reduced upon adsorption on the surface [66]). Analogous isomerization-mediated pathways

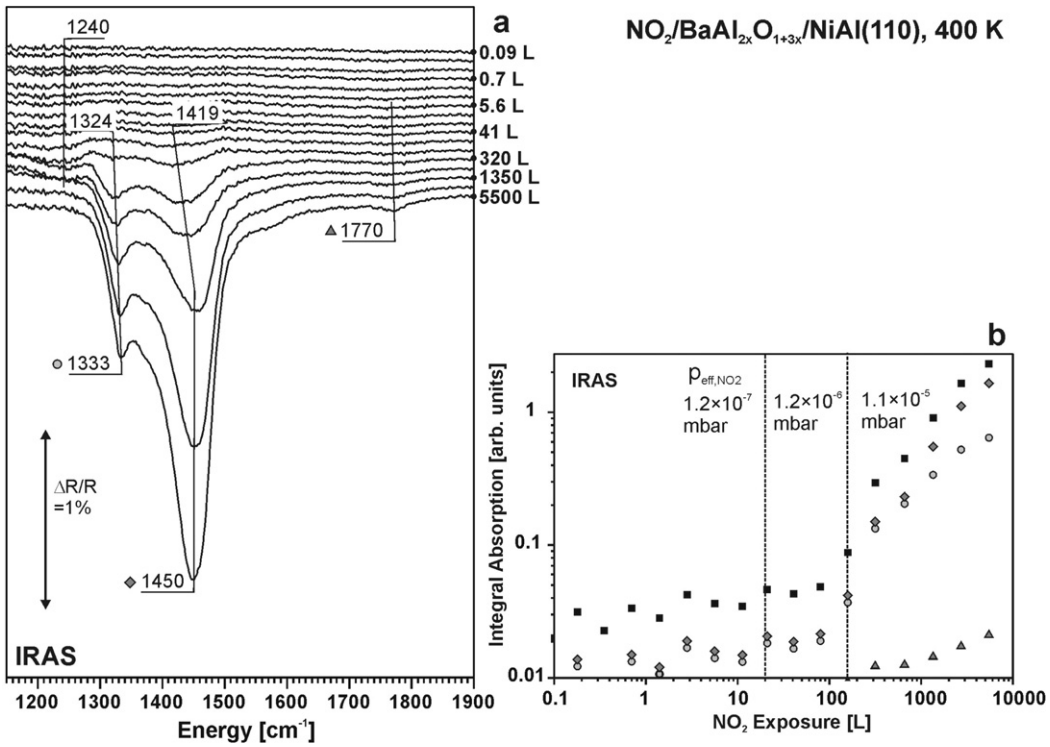


**Fig. 7.** Interaction of $NO_2$ with the $BaAl_{2x}O_{1+3x}$ nanoparticles supported on $Al_2O_3$/NiAl(110) at 400 K: (a) IR reflection absorption spectra of the NO stretching frequency region as a function of $NO_2$ exposure; (b) integral absorption of the most prominent spectral features (gray symbols) and total absorption in the N–O stretching frequency region (black symbols) as a function of $NO_2$ exposure.

have been suggested for other surface reactions involving $N_2O_4$ at low temperature (see e.g. [47]). Venkov et al. invoked a similar disproportionation mechanism in the case of the reaction of NO and $O_2$ on $Al_2O_3$ and were able to spectroscopically detect the $NO^+$ species formed [67].

The drastic decrease of the nitrate formation rate at higher temperatures may be ascribed to a change in reaction mechanism, which is associated to the absence of $N_2O_4$ dimers under these conditions. The most straightforward assumption would imply a switch in mechanism from a cooperative process involving two $NO_2$ entities to a non-cooperative mechanism involving a single $NO_2$ species only. This hypothesis is supported by the change in the product spectrum yielding nitrites as the only initial product at 300 K. Different cooperative and non-cooperative adsorption and reaction mechanisms for $NO_2$ on BaO and other alkaline earth metals have theoretically investigated and discussed by Schneider and coworkers [32,64] and by Grönbeck et al. [30,31]. In case of the non-cooperative adsorption pathway, formation of the surface nitrite may occur via Lewis acid/base interaction and subsequent electron transfer. The process would initially lead to generation of an electron hole, localized on a surface oxygen atom (see [64]):

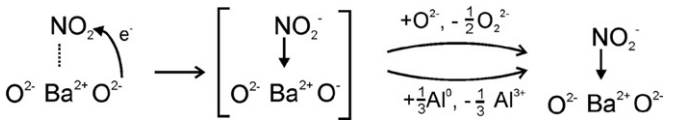


(2)

For the present model system, we may invoke two reaction channels via which this excess charge may be annihilated. The first process would be the formation of peroxide species and/or the generation of molecular oxygen. It is well known that such peroxides are easily formed on BaO [23,29] and the corresponding species have recently been observed direct by STM [68]. The second pathway, which is restricted to thin film model systems, involves further oxidation of the substrate. In the present case, Al originating from the NiAl substrate may be oxidized, leading to further growth of the $Al_2O_3$ support layer. The latter process has been directly observed during reaction at 300 K by HR-PES [36]. It is expected that the contribution of the latter reaction channel decreases with increasing thickness of the oxide layer.

### 3.4. Reaction of $NO_2$ with $BaAl_{2x}O_{1+3x}$ nanoparticles at elevated temperatures (400–600 K)

In order to probe the reactivity of the $BaAl_{2x}O_{1+3x}$ nanoparticles as a function of surface temperature, a series of temperature-dependent experiments was performed, applying the standard experimental procedure outlined in Section 3.2. The sample was maintained at constant temperatures between 400 and 600 K, while being exposed to pulses of $NO_2$ of different duration and intensity. Each pulse was followed by acquisition of an IR spectrum at the respective temperature. In order to reduce data acquisition times, the number of pulses was restricted to a minimum. The corresponding IRAS spectra for the N–O stretching frequency region are displayed in Figs. 7, 8, and 9 for reaction temperatures of 400, 500, and 600 K, respectively. The integral intensity of several individual features as a function of exposure is displayed in part b of the corresponding figures. A direct comparison between the spectra in the limit of large exposures is provided in Fig. 10a. In addition, the total integral absorption in the N–O stretching frequency region as a function of reaction temperature and $NO_2$ exposure is displayed in Fig. 10b.

In comparison to the experiments at 300 K, a drastically different behavior is observed. The most prominent dissimilarity is related to the integral absorption, which increases by at least a factor of three in the temperature interval between 300 and 400 K. In the temperature region between 400 and 600 K, on the other hand, the intensity of the bands in the high exposure limit (~6000 L

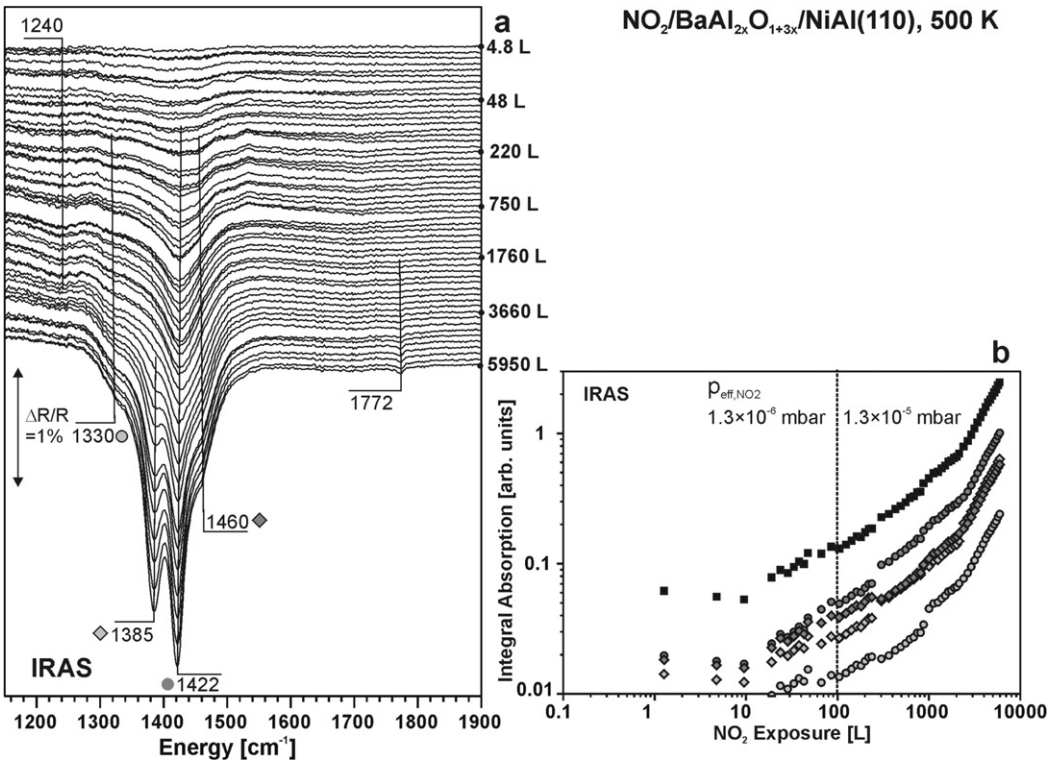


**Fig. 8.** Interaction of $NO_2$ with the $BaAl_{2x}O_{1+3x}$ nanoparticles supported on $Al_2O_3$/NiAl(110) at 500 K: (a) IR reflection absorption spectra of the NO stretching frequency region as a function of $NO_2$ exposure; (b) integral absorption of the most prominent spectral features (gray symbols) and total absorption in the N–O stretching frequency region (black symbols) as a function of $NO_2$ exposure.

$NO_2$) remains similar (see Fig. 10b), whereas the spectral features themselves undergo drastic changes (see Fig. 10a).

At 400 K (Fig. 7), the behavior in the low exposure limit is similar to reaction at 300 K. At 10 to 100 L $NO_2$, a broad feature around 1250 $cm^{-1}$ appears, followed by weak bands around 1330 and 1420 $cm^{-1}$. With increasing exposure, the feature at 1250 $cm^{-1}$ decreases again, whereas the bands at 1330 and 1420 $cm^{-1}$ rapidly gain intensity. In the exposure region between 1000 and 5000 L, the relative intensity of the two latter bands changes and the high-frequency component undergoes a blue shift to 1450 $cm^{-1}$. Finally, the peak at 1450 $cm^{-1}$ becomes the dominating band in the IR spectrum. At the highest exposure, shoulders on both sides of the band at 1450 $cm^{-1}$ develop, i.e. at around 1380 and at 1570 $cm^{-1}$. In addition, a weak feature appears in the high frequency region at 1770 $cm^{-1}$.

According to the discussion in Section 3.3, we assign the band at 1250 $cm^{-1}$ to surface nitrites on BaO. Similarly as for reaction at 300 K, the low intensity of the nitrite band indicates an orientation parallel to the surface. In addition, the nitrite coverage may be somewhat lower as compared to 300 K because of more efficient conversion to the nitrate. Still, it should be pointed out that both at 300 K and at elevated temperatures, nitrites are the primary product, as we have recently shown in a combined IRAS/XPS study [28]. The bands in the region between 1300 and 1500 $cm^{-1}$ are again attributed to Ba nitrates. According to the literature (see discussion in Section 3.3), the most straightforward assignment of the features around 1320 and 1420 $cm^{-1}$ would be to monodentate nitrates. However, taking into account the intensity arguments outlined above (see also [59]) a somewhat different picture evolves. At low coverage, the intensities of both components of $\nu_{as}(NO_3^-)$ are similar, pointing toward a mixture of different coordination geometries. At high exposure, the high frequency component dominates, rather suggesting to preferential formation of bridging nitrates. In addition, the very high intensity of the nitrate peak in the high exposure limit suggests that nitrate formation proceeds beyond the surface, and aggregates of (multilayer) ionic nitrates may be formed as well. Such ionic Ba nitrates are typically identified by a characteristic band around 1380 $cm^{-1}$ [49,57]. In the present case, the large width of the bands points to a rather poorly defined local structure, impeding clear identification of corresponding spectral features. Also, the origin of the emerging band at 1570 $cm^{-1}$ is unclear. Bands in this region have been observed on powder NSR catalysts as well and may involve coordination of nitrates not only to $Ba^{2+}$ but also to $Al^{3+}$ sites [54]; a hypothesis which appears not unlikely in view of the high surface concentration of $Al^{3+}$ ions within the $BaAl_{2x}O_{1+3x}$ particles. Finally, different assignments have been invoked with respect to the weak high frequency feature at 1770 $cm^{-1}$ [30]. In principle, one may expect metal nitrosyls to show bands in this range, and the formation of nitrosyls has indeed been observed on related model surfaces [69]. However, the present peak at 1770 $cm^{-1}$ clearly follows the intensity behavior of the nitrate bands and is most probably directly related to this species. Therefore, we assign this feature to a combination band of the symmetric NO stretching mode ($\nu_1$ or $\nu_s(NO_3^-)$) and the in-plane deformation ($\nu_4$), which is also observed for the $Ba(NO_3)_2$ single crystal [70].

If we now proceed to the reaction at 500 K (see Fig. 8), we find that even at lowest exposure the bands between 1300 and 1500 $cm^{-1}$ dominate over the low frequency features around 1240 $cm^{-1}$. Initially, peaks around 1420 to 1460 $cm^{-1}$ appear, together with weaker bands around 1330 and 1250 $cm^{-1}$. Above 2000 L, two very intense and narrow peaks start to grow at 1422 and 1385 $cm^{-1}$. In the high coverage limit, these two bands dominate the spectrum together with shoulders at 1330 and 1460 $cm^{-1}$ and the weak high frequency band at 1770 $cm^{-1}$.

In accordance with the above discussion we attribute the feature at 1250 $cm^{-1}$ to surface nitrites and the bands at 1300 and 1450 $cm^{-1}$ to the split $\nu_{as}(NO_3^-)$ of surface nitrates. In spite of

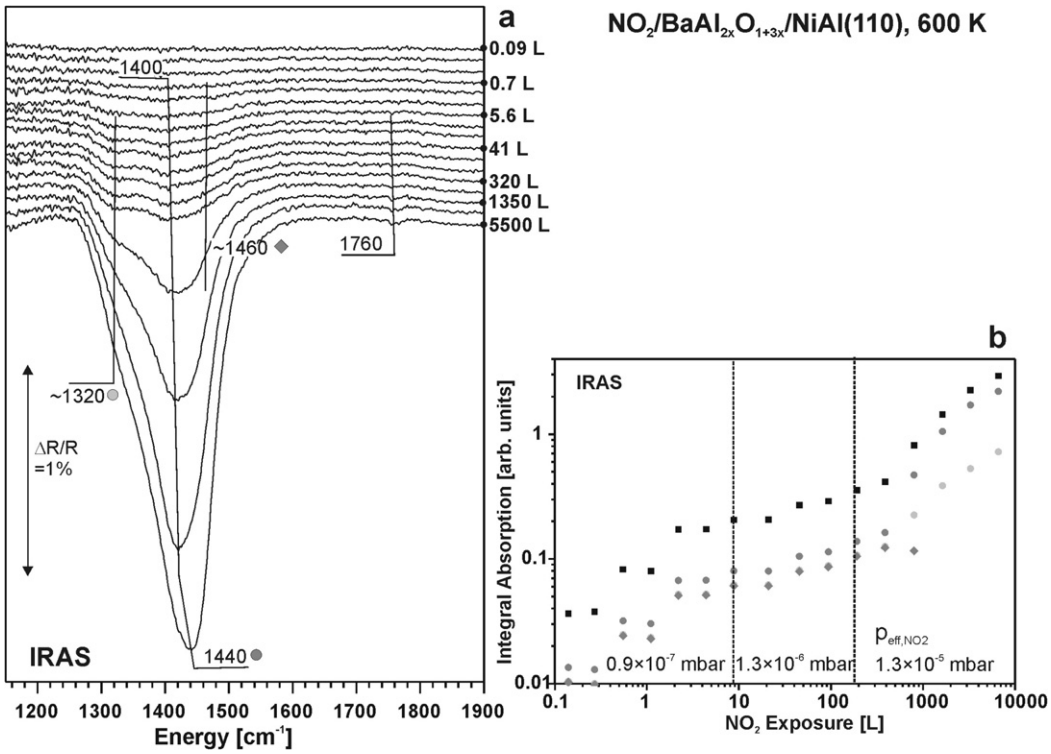


**Fig. 9.** Interaction of $NO_2$ with the $BaAl_{2x}O_{1+3x}$ nanoparticles supported on $Al_2O_3$/NiAl(110) at 600 K: (a) IR reflection absorption spectra of the NO stretching frequency region as a function of $NO_2$ exposure; (b) integral absorption of the most prominent spectral features (gray symbols) and total absorption in the N–O stretching frequency region (black symbols) as a function of $NO_2$ exposure.

the dominance of the nitrate features, recent combined IRAS/XPS studies have clearly shown that even at 500 K, surface nitrites are the initial products of the reaction [28]. However, these nitrites are more efficiently converted into nitrates at elevated temperature [28], and the surface nitrates dominate the vibrational spectrum due to the low sensitivity of the nitrite in the IRAS experiment. It is noteworthy that the nitrite band vanishes completely at large exposure, indicating facile conversion of nitrites into nitrates (compare [28]). The intensity ratio between the two nitrate bands suggests the preferential formation of bridging nitrates (see Section 3.3). The two bands which appear simultaneously at 1422 and 1385 $cm^{-1}$ are assigned to ionic nitrates. As confirmed by theory, the reduced splitting between the two components of $\nu_{as}(NO_3^-)$ is a characteristic spectroscopy feature of the ionic nitrate species [59]. In general, the splitting is the consequence of the lifted degeneracy between the two components of $\nu_{as}(NO_3^-)$, which could be caused either by distortion of the $C_{3v}$ symmetry of the ion or by interaction with the surrounding electrostatic potential. In the case of a $Ba(NO_3)_2$ single crystal, the crystal field leads to a splitting of $\nu_{as}(NO_3^-)$ yielding two IR active components separated by 70 $cm^{-1}$ [70,71]. DFT calculations for adsorption of single $NO_3^-$ species on BaO clusters yield splittings around 100 $cm^{-1}$ [59]. The smaller splitting observed in the present study and the fact that the splitting is independent of the amount of ionic nitrate formed suggests a relatively weak interaction with the surface and may indicate that this interaction is of a more local type, e.g. occurs with a single or well defined ensemble of ions. Moreover, the sharpness of the two ionic nitrate bands suggests the formation of a phase with an at least locally well-defined structure.

Proceeding to reaction at 600 K (Fig. 9), no features in the range around 1250 $cm^{-1}$ are observed anymore. Broad bands around 1320 and 1400 $cm^{-1}$ appear in the low exposure region, with the high frequency band becoming very strong and shifting to 1440 $cm^{-1}$ for large exposures. In addition, very weak features around 1760 $cm^{-1}$ are detected.

Considering the reaction behavior of 600 K, we have to keep in mind that under these conditions we are approaching the decomposition temperature of Ba nitrates (compare [38,54,56]). The shoulder at 1320 $cm^{-1}$ is assigned to the low frequency component of the split nitrate mode (see Sections 3.3 and 3.3), whereas the huge intensity around 1400 $cm^{-1}$ in the high coverage limit points toward multilayer formation of ionic nitrates (overlapping with the $\nu_{as}(NO_3^-)$ high frequency component of surface nitrates). However, the features in the range between 1400 and 1500 $cm^{-1}$ are very broad and no individual spectral components can be differentiated, in sharp contrast to the situation at 500 K. This observation points to the formation of a less well-defined local structure of the ionic nitrate layer, in comparison to the reaction at 500 K. It is noteworthy that the initial formation of nitrites is not observed anymore. This finding indicates that nitrite species are efficiently converted to nitrates, either via decomposition under release of NO and oxidation of surface nitrite to nitrate or via rapid reaction with $NO_2$ from the gas phase.

## 4. Conclusion

In summary, we have studied the interaction of $NO_2$ with $Al_2O_3$/NiAl(110) in the temperature region between 100 and 300 K as well as the interaction of $NO_2$ with $BaAl_{2x}O_{1+3x}$ nanoparticles supported on $Al_2O_3$/NiAl(110) between 100 and 600 K. Morphology, growth and chemical composition of the nanoparticles were previously characterized by STM and HR-PES. In the present study we focus on larger nanoparticles containing in average approximately 600 $Ba^{2+}$ ions per particle.

We have performed systematic measurements of the adsorption and reaction behavior applying TR-IRAS in combination with MB dosing. In fully remote-controlled sequences, a broad coverage range between approximately $10^{-1}$ and $10^4$ L was probed. We summarize the main observations and conclusions as follows:

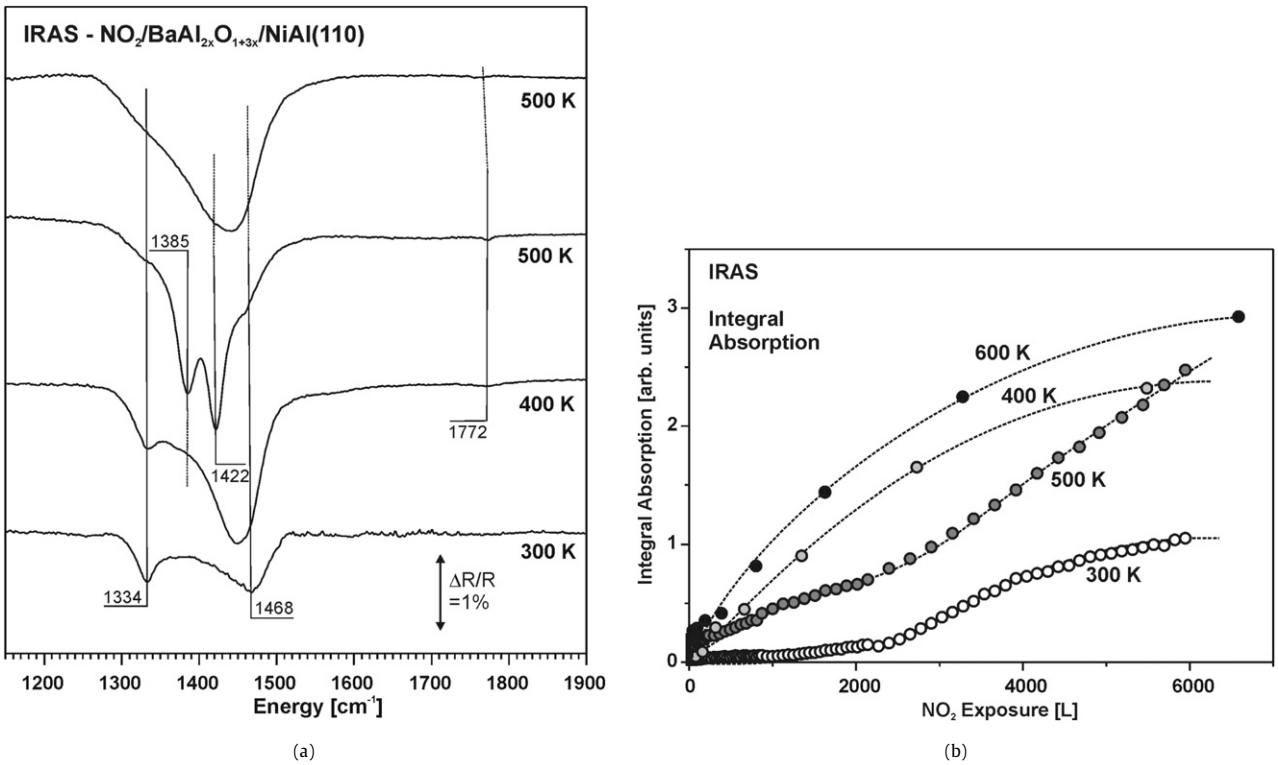


**Fig. 10.** Temperature dependence of the reaction of $NO_2$ with the $BaAl_{2x}O_{1+3x}$ nanoparticles on $Al_2O_3$/NiAl(110): (a) IR reflection absorption spectra after the maximum exposure to $NO_2$ applied in this study (approximately 6000 L, see Figs. 6–9); (b) comparison of the total intensity of the bands in the N–O stretching frequency region as a function of reaction temperature and $NO_2$ exposure.

(1) On $Al_2O_3$/NiAl(110) at 100 K, $NO_2$ adsorbs under formation of the $D_{2h}$ dimer ($N_2O_4$), without any indication for other byproducts. The bands observed can be attributed to the $\nu_s$(ONO) and $\nu_{as}$(ONO) modes of the dimer with a characteristic splitting in both regions. It is shown that monolayer and thin multilayer structures show a characteristic molecular orientation with respect to the surface, whereas this orientation is lost upon formation of thick multilayer structures.

(2) Upon interaction of $NO_2$ with $Al_2O_3$/NiAl(110) at 300 K, there are no indications for molecularly adsorbed species. The alumina film, however, is not inert with respect to reaction with $NO_2$. Initially, we observe a slow reaction leading to the formation of surface nitrites, which is followed by formation of bridging nitrates. At higher exposure, a second bridging nitrate species is formed at a substantially higher rate. It is suggested that the increasing rate of nitrate formation is related to a structural transformation of the surface, induced by the surface reaction itself.

(3) For reaction of $NO_2$ with the $BaAl_{2x}O_{1+3x}$ nanoparticles at 300 K, initial formation of surface nitrites is observed. These species are preferentially oriented parallel to the surface (nitrito or nitro-nitrito). At higher exposure, surface nitrates are formed at substantially lower rate. There are indications for the presence of both monodentate and bridging nitrates, with their relative abundance sensitively depending on coverage. The rate of nitrate formation accelerates during reaction, suggesting a reaction-induced surface restructuring process. At 300 K, the reaction is restricted to the surface of the BaO particles and no ionic nitrites or nitrates are detected.

(4) For the reaction of $NO_2$ with the $BaAl_{2x}O_{1+3x}$ nanoparticles at 100 K, a high reaction probability is observed and the initial product spectrum changes to the simultaneous formation of both nitrites and nitrates. It is concluded that at low temperature the reaction proceeds via a cooperative mechanism leading to the formation of nitrite–nitrate pairs. We suggest that the highly efficient cooperative mechanism involves molecular adsorption of $NO_2$, dimerization and disproportionation of the dimer. At higher temperature, there is no formation of surface dimers and the reaction switches to a non-cooperative mechanism with the surface nitrite representing the only initial product. The non-cooperative channel is characterized by a substantially lower reaction probability.

(5) The interaction of $NO_2$ with the $BaAl_{2x}O_{1+3x}$ nanoparticles shows very strong temperature dependence in the temperature range between 400 and 600 K. At 400 K and above, the reaction is not restricted to the particle surface but may also involve multilayer formation of nitrates. Although the nitrite remains the initial product at low exposure, conversion to the nitrate becomes increasingly more efficient until no nitrites can be detected anymore for reaction temperatures around 600 K. The vibrational signature of the nitrates characteristically depends on the reaction temperature. In a narrow temperature interval around 500 K the reaction leads to the formation of ionic nitrates in a well defined local arrangement. Structurally less well-defined aggregates are generated at lower or higher temperature.

The experiments show that several elementary steps involved in the $NO_x$ storage process can be successively probed via model experiments in an UHV environment. This includes both the initial stages of nitrite and nitrate formation and the formation of multilayer nitrates. In particular, the present study provides insights into the detailed mechanism of nitrate and nitrite formation and may help to resolve some of the contradictory results which are presently found in the literature. Due to the large variations in reaction probability for the different steps, however, the model experiments require a systematic approach and large $NO_2$ exposures. The current experiments on nanostructured storage materials pro-

vide a basis for future investigations on the elementary mechanism and kinetics of reactions on complete $NO_x$ model storage catalysts, containing both Ba-based storage materials and noble metal components.

## Acknowledgments

The present project was performed in co-operation and supported by the Umicore AG&Co. KG (Automotive Catalysts). We thank Friedemann Rohr (Umicore AG&Co. KG, Hanau) for helpful discussions. The authors are particularly grateful to Zhihui Qin, Shamil Shaikhutdinov and Hans-Joachim Freund (FHI Berlin) for providing STM images and facilities. The support of Karsten Meyer, Matthias Moll, Marc Gärtner and Carola Vogel (University Erlangen) with respect to the required local glove box facilities is acknowledged. The authors thank Henrik Grönbeck and Konstantin M. Neyman for fruitful cooperations and discussions. We acknowledge financial support of the DFG (LI 909/7-1), DAAD (PPP, Acciones Integradas Hispano-Alemanas), EU (COST D-41), the Fonds der Chemischen Industrie and the "Zerweck Fonds" (Universitätsbund Erlangen-Nürnberg).

## References

[1] J.M. Thomas, W.J. Thomas, Principle and Practice of Heterogeneous Catalysis, VCH, Weinheim, 1997.
[2] R. Di Monte, J. Kaspar, Top. Catal. 28 (2004) 47.
[3] R.M. Heck, R.J. Farrauto, S.T. Gulati, Catalytic Air Pollution Control—Commercial Technology, John Wiley & Sons, 2002.
[4] N. Takahashi, H. Shinjoh, T. Iijima, T. Suzuki, K. Yamazaki, K. Yokota, H. Suzuki, N. Miyoshi, S. Matsumoto, T. Tanizawa, T. Tanaka, S. Tateishi, K. Kasahara, Catal. Today 27 (1996) 63.
[5] W.S. Epling, L.E. Campbell, A. Yezerets, N.W. Currier, J.E. Parks II, Catal. Rev. 46 (2004) 163.
[6] F. Rohr, S.D. Peter, E. Lox, M. Kögel, A. Sassi, L. Juste, C. Rigaudeau, G. Belot, P. Gelin, M. Primet, Appl. Catal. B Environ. 56 (2005) 201.
[7] I. Nova, L. Castoldi, F. Prinetto, V. DalSanto, L. Lietti, E. Tronconi, P. Forzatti, G. Ghiotti, R. Psaro, S. Recchia, Top. Catal. 30/31 (2004) 181.
[8] M. Piacentini, R. Stroebel, M. Maciejewski, S.E. Pratsinis, A. Baiker, J. Catal. 243 (2006) 43.
[9] L. Castoldi, R. Matarrese, L. Lietti, P. Forzatti, Appl. Catal. B Environ. 64 (2006) 25.
[10] R.G. Tonkyn, R.S. Disselkamp, C.H.F. Peden, Catal. Today 114 (2006) 94.
[11] J. Dawody, I. Tonnies, E. Fridell, M. Skoglundh, Top. Catal. 42–43 (2007) 183.
[12] H.-J. Freund, M. Bäumer, J. Libuda, T. Risse, G. Rupprechter, S. Shaikhutdinov, J. Catal. 216 (2003) 223.
[13] J. Libuda, H.-J. Freund, Surf. Sci. Rep. 57 (2005) 157.
[14] C.R. Henry, Surf. Sci. Rep. 31 (1998) 231.
[15] M. Baumer, J. Libuda, K.M. Neyman, N. Rosch, G. Rupprechter, H.-J. Freund, Phys. Chem. Chem. Phys. 9 (2007) 3541.
[16] M.S. Chen, D.W. Goodman, Acc. Chem. Res. 39 (2006) 739.
[17] C.T. Campbell, S.C. Parker, D.E. Starr, Science 298 (2002) 811.
[18] V.P. Zhdanov, B. Kasemo, Surf. Sci. Rep. 39 (2000) 25.
[19] P. Stone, M. Ishii, M. Bowker, Surf. Sci. 537 (2003) 179.
[20] M. Bowker, P. Stone, R. Smith, E. Fourre, M. Ishii, N.H. de Leeuw, Surf. Sci. 600 (2006) 1973.
[21] A. Tsami, F. Grillo, M. Bowker, R.M. Nix, Surf. Sci. 600 (2006) 3403.
[22] E. Ozensoy, C.H.F. Peden, J. Szanyi, J. Phys. Chem. B 110 (2006) 17001.
[23] E. Ozensoy, C.H.F. Peden, J. Szanyi, J. Phys. Chem. B 110 (2006) 17009.
[24] E. Ozensoy, C.H.F. Peden, J. Szanyi, J. Phys. Chem. B 109 (2005) 15977.
[25] E. Ozensoy, C.H.F. Peden, J. Szanyi, J. Phys. Chem. B 110 (2006) 8025.
[26] E. Ozensoy, C.H.F. Peden, J. Szanyi, J. Catal. 243 (2006) 149.
[27] P.J. Schmitz, R.J. Baird, J. Phys. Chem. B 106 (2002) 4172.
[28] A. Desikusumastuti, M. Happel, K. Dumbuya, T. Staudt, M. Gottfried, H.-P. Steinrück, J. Libuda, J. Phys. Chem. C, in press.
[29] C. Hess, J.H. Lunsford, J. Phys. Chem. B 106 (2002) 6358.
[30] P. Broqvist, H. Grönbeck, E. Fridell, I. Panas, J. Phys. Chem. B 108 (2004) 3523.
[31] H. Grönbeck, P. Broquist, I. Panas, Surf. Sci. 600 (2006) 403.
[32] M. Miletic, J.L. Gland, K.C. Hass, W.F. Schneider, J. Phys. Chem. B 107 (2003) 157.
[33] W.F. Schneider, J. Chem. Phys. B 108 (2004) 273.
[34] C.-W. Yi, J.H. Kwak, J. Szanyi, J. Phys. Chem. C 111 (2007) 15299.
[35] C.-W. Yi, J.H. Kwak, C.H.F. Peden, H. Wang, J. Szanyi, J. Phys. Chem. C 111 (2007) 14942.
[36] T. Staudt, A. Desikusumastuti, M. Happel, E. Vesselli, A. Baraldi, S. Gardonio, S. Lizzit, F. Rohr, J. Libuda, submitted for publication.
[37] D.H. Kim, J.H. Kwak, J. Szanyi, S.D. Burton, C.H.F. Peden, Appl. Catal. B Environ. 72 (2007) 233.
[38] A. Desikusumastuti, M. Laurin, M. Happel, Z. Qin, S. Shaikhutdinov, J. Libuda, Catal. Lett. 121 (2008) 311.
[39] R.M. Jaeger, H. Kuhlenbeck, H.-J. Freund, M. Wuttig, W. Hoffmann, R. Franchy, H. Ibach, Surf. Sci. 259 (1991) 235.
[40] J. Libuda, F. Winkelmann, M. Bäumer, H.-J. Freund, T. Bertrams, H. Neddermeyer, K. Müller, Surf. Sci. 318 (1994) 61.
[41] G. Kresse, M. Schmid, E. Napetschnig, M. Shishkin, L. Köhler, P. Varga, Science 308 (2005) 1440.
[42] R.M. Jaeger, J. Libuda, M. Bäumer, K. Homann, H. Kulenbeck, H.-J. Freund, J. Electron Spectrosc. Relat. Phenom. 64/65 (1993) 217.
[43] M. Bäumer, H.-J. Freund, Prog. Surf. Sci. 61 (1999) 127.
[44] M. Schmid, M. Shishkin, G. Kresse, E. Napetschnig, P. Varga, M. Kulawik, N. Nilius, H.-P. Rust, H.-J. Freund, Phys. Rev. Lett. 97 (2006) 046101.
[45] H. Rieley, D.P. McMurray, S. Haq, J. Chem. Soc. Faraday Trans. 92 (1996) 933.
[46] J. Wang, E.E. Koel, J. Phys. Chem. B 102 (1998) 8573.
[47] J. Wang, B.E. Koel, Surf. Sci. 436 (1999) 15.
[48] S. Sato, D. Yamaguchi, K. Nakagawa, Y. Inoue, A. Yabushita, M. Kawasaki, Langmuir 16 (2000) 9533.
[49] K.I. Hadjiivanov, Catal. Rev.-Sci. Eng. 42 (2000) 71.
[50] F.M. Hoffmann, Surf. Sci. Rep. 3 (1983) 107.
[51] A.L. Goodman, T.M. Miller, V.H. Grassian, J. Vac. Sci. Technol. A 16 (1998) 2585.
[52] C. Paze, G. Gubitosa, S.O. Giacone, F.X. Llabres i Xamena, A. Zecchina, Top. Catal. 30/31 (2004) 169.
[53] T. Szailer, J.H. Kwak, D.H. Kim, J.C. Hanson, C.H.F. Peden, J. Szanyi, J. Catal. 239 (2006) 51.
[54] B. Westerberg, E. Fridell, J. Mol. Catal. A Chem. 165 (2001) 249.
[55] F. Prinetto, G. Ghiotti, I. Nova, L. Lietti, E. Tronconi, P. Forzatti, J. Phys. Chem. B 105 (2001) 12732.
[56] C. Sedlmair, K. Seshan, A. Jentys, J.A. Lercher, J. Catal. 214 (2003) 308.
[57] K. Hadjiivanov, V. Bushev, M. Kantcheva, D. Klissurski, Langmuir 10 (1994) 464.
[58] W.S. Brown, D.A. King, J. Phys. Chem. B 104 (2000) 2578.
[59] A. Desikusumastuti, T. Staudt, H. Grönbeck, J. Libuda, J. Catal. 255 (2008) 127.
[60] E. Fridell, M. Skoglundh, B. Westerberg, S. Johansson, G. Smedler, J. Catal. 183 (1999) 196.
[61] C. Hess, J.H. Lunsford, J. Phys. Chem. B 107 (2003) 1982.
[62] P. Broquist, H. Grönbeck, E. Fridell, I. Panas, J. Phys. Chem. B 108 (2004) 3523.
[63] P. Hollins, Surf. Sci. Rep. 16 (1992) 51.
[64] W.F. Schneider, J. Phys. Chem. B 108 (2004) 273.
[65] A.S. Pimentel, F.C.A. Lima, A.B.F.d. Silva, J. Phys. Chem. A 111 (2007) 2913.
[66] A.J. Vosper, J. Chem. Soc. A (1970) 625.
[67] T. Venkov, K. Hadjiivanov, D. Klissurski, Phys. Chem. Chem. Phys. 4 (2002) 2443.
[68] M. Bowker, M. Cristofolini, M. Hall, E. Fourre, F. Grillo, E. McCormack, P. Stone, M. Ishii, Top. Catal. 42–43 (2007) 341.
[69] S. Schauermann, V. Johánek, M. Laurin, J. Libuda, H.-J. Freund, Chem. Phys. Lett. 381 (2003) 298.
[70] M.H. Brooker, D.E. Ernst, G.E. Boyd, J. Chem. Phys. 53 (1970) 1083.
[71] P.G. Zverev, T.T. Basiev, V.V. Osiko, A.M. Kulkov, V.N. Voitsekhovskii, V.E. Yakobson, Opt. Mater. 11 (1999) 315.